Computer Science Journal of Moldova, vol.**22**, no.2(65), 2014

Optic Disc Identification Methods for Retinal Images

Invited Article

Florin Rotaru, Silviu Ioan Bejinariu, Cristina Diana Niţă, Ramona Luca, Camelia Lazăr

Abstract

Presented are the methods proposed by authors to identify and model the optic disc in colour retinal images. The first three our approaches localized the optic disc in two steps: a) in the green component of RGB image the optic disc area is detected based on texture indicators and pixel intensity variance analysis; b) on the segmented area the optic disc edges are extracted and the resulted boundary is approximated by a Hough transform. The last implemented method identifies the optic disc area by analysis of blood vessels network extracted in the green channel of the original image. In the segmented area the optic disc edges are obtained by an iterative Canny algorithm and are approximated by a circle Hough transform.

Keywords: optic disc, retinal images, vessel segmentation, Hough transform.

1 Introduction

Proposed in the last years, there is a huge literature on automatic analysis of retinal images, the optic disc evaluation being part of this work. The recognition and assessment of optic disc in retinal images are important tasks to evaluate retina diseases as diabetic macular edema, glaucoma, etc. The uneven quality and diversity of the acquired retinal images and the large variations between individuals made the

automatic analysis a strongly context dependent task. Even so valuable methods were proposed and the authors have reported their results lately using public retinal images databases as DRIVE (40 images), DIARETDB1 (89 images) or STARE (402 images).

Part of the proposed techniques, called bottom-up methods, first locate the optic disc and then starting from that area track the retinal vessels and do the required measurements [1], [2], [3], [8]. There is another approach of retinal image analysis that tracks the retinal vessels and gets the optic disc as the root of the vessels tree. The second one is called top-down approach [4], [5], [7], [17]. Besides these two trends, there are mixed approaches, independently detecting the optic disc centre and retinal vessels, as the ones proposed in [15], [23]. In these ones the blood vessel network analysis is combined with other methods to locate optic disc area.

A bottom-up technique is presented in [1]. The optic disc recognition and modelling were done in two steps. The first one locates the optic disc area using a voting procedure. There were implemented three methods: the maximum difference method that computes the maximum difference between the maximum and minimum grey levels in working windows, the maximum variance method and frequency low pass filter method. The green channel of the RGB input image was used. The first method filters the image using a 21×21 median filter and then for each pixel in the filtered image the difference between the maximum and minimum grey levels in a 21×21 window centred on the current pixel is computed. The pixel with the maximum difference is chosen optic disc centre candidate. Second method calculates the statistical variance for every pixel of the green channel using a 71×71 window. Then, the blue channel image is binarized by Otsu technique. The pixel in the green channel with the maximum statistical variance and having at least 10 white neighbours pixels in a 101×101 area centred on it but in the blue binarized channel is proposed as disc centre. The third voting method transforms the green channel from spatial domain to frequency domain, by a Fourier transform. The magnitude image of the transform is filtered using a Gaussian low-pass filter and the result image is transformed back to the spatial domain. The bright-

est pixel in result image is taken as the third optic disc centre candidate. Finally the voting procedure chooses the estimated disc centre from the three candidates: 1) if all three candidates are close to their centre of mass, the centre of mass is proposed as an approximate disc centre; 2) if only two from three candidates are close to the centre of mass of all three points, the centre of mass of these two candidates is chosen; 3) if all candidates are far apart from their centre of mass, the candidate proposed by the second method is chosen, the most reliable considered by the authors.

Part of this optic disc area segmentation was also implemented in our first system to process retinal images.

In the second step of the whole methodology proposed in [1] a 400×400 window is centred on the estimated disc centre, and extracted from green and red channels of the original image. A morphological filter is employed in [6] to erase the vessels in the new window and a Prewitt edge detector is then applied. Then, by the same Otsu technique, the image is binarized. The result is cleaned by morphological erosion and finally a Hough transform is applied to get the final optic disc boundary. The boundary with the best fitting from the two channels is chosen. The authors report for 1200 retinal images a score of 100% for approximated localisation and a score of 86% for final optic disc localisation.

Another bottom up approach to locate optic disc area was proposed in [8]. The method combines two algorithms: a pyramidal decomposition using Haar wavelet transform and an optic disc contour detection based on Haussdorf distance. Areas, usually white patches that might disturb the right disc area detection are eliminated during the pyramid synthesis. In the end, the low resolution level contains only the useful information. Finally the disc is selected from ten optic disc candidates.

In [3] another automatic optic disc detection was proposed based on majority voting for a set of optic disc detectors. There were employed five methods to detect optic disc centre: pyramidal decomposition [8], edge detection [8], entropy filter [14], fuzzy model [5] and Hough transform [10]. Each of the five methods is applied on the whole working image. A circular template is fit on each pixel in the initial image to

count the outputs of these algorithms that fall within the radius. The circle with the maximum number of optic disc detector outputs in its radius is the chosen area to refine the optic disc detection. An improved version of the voting method was proposed in [2].

From the top down methods the one proposed in [4] detects the retinal vessels convergence using a voting-type algorithm named fuzzy convergence. In another paper [5], in a first step there are identified the four main vessels in the image. Then the four branches are modelled by two parabolas whose common vertex is identified as the optic disc centre.

Another top down approach is proposed in [17]. The blood vessel network is segmented after a sequence of morphological operations:

a) the bright areas, associated with diabetic lesions, are removed applying a morphological operator to detect regional minima pixels and then the resulted image is reconstructed by dilation;

b) the result background image is enhanced by a morphological contrast operation and then a Gaussian filter is applied;

c) the elongated low intensities regions, associated with vascular tree, are extracted with a top-hat by closing operator;

d) the maximum of openings are retained for a structuring element of 80 pixels long segment and 24 orientations. These are the main branches of the vessels tree;

e) the vascular tree is then estimated by reconstruction by dilation using the result image from step d) as marker image and the result image from step c) as mask element;

f) the grey level image resulted in previous step is binarized using a morphological operator to detect regional minima pixels as in step a). The result is complemented;

g) the skeleton of the vessel tree is obtained in the binary image by morphological operation;

h) the useless short vessels branches are eliminated by a 20 step pruning operation.

In the resulted vessel tree image a point close to optic disc is calculated: a) the holes of the vessel network are filled; b) the tree branches are thinned; c) a recursive pruning operation is applied until no more reduction is possible, so only the main parabolic branch remains. The mass centre of the parabolic branch is considered the point closest to the optic disc.

In [17] other optic disc detection methods taxonomy is proposed. There is identified a first group of methods, [7], [18 – 21], that localizes the optic disc centre as the convergence point of the main blood vessels. However, these methods can be assimilated to the top-down category. From the second category group identified in [17], M. Niemeijer [23] uses a mixed algorithm combining the vessel network analysis and other segmentation method to locate optic disc area. The rest of the methods proposed in the second group of papers, [13], [22], [24 – 28] can be assimilated to the bottom-up methods. For two of these papers, [27] and [28], the main purpose is the exudate detection, so the optic disc detection and elimination are mandatory. While in [28] the optic disc area is identified using morphological operators, in [27], besides morphological filtering techniques, the watershed transformation is used. Another approach [22] from the second group identifies the optic disc using specialized template matching and segmentation by a deformable contour model. In [25] a genetic algorithm is proposed to localize the optic disc boundary. In [26] the authors utilize texture descriptors and a regression based method to find the most likely circle fitting the optic disc.

Most of the papers mentioned in the taxonomy proposed in [17] report very good results of detecting optic disc area for images from DRIVE or DIARETDB1 database or both.

2 Optic disc area segmentation methods

To locate the optic disc area we started following a similar methodology as the one proposed in [1]. In the first attempt tests have been done on 720×576 RGB retinal images [11], provided by our collaborators from Grigore T. Popa University of Medicine and Pharmacy, Iaşi, Romania

(UMP). From the three methods of the voting procedure presented in [1] we obtained good optic disc area localisation with a modified Low-Pass Filter Method and the Frequency Low Pass Filter Method.

The first method was implemented as in [1]. The green channel of the input image was transformed in frequency domain and on the image of the magnitude of the FFT transform a Gaussian low-pass filter was applied:

$$H(u,v) = \exp\left(-\frac{D^2(u,v)}{2D_0^2}\right), \tag{1}$$

where $D(u,v)$ is the Euclidean distance from point (u,v) to the origin of frequency domain and D_0 is the cutoff frequency, of 25 Hz. The result was transformed back to the spatial domain and the brightest pixel of the result image was chosen as an optic disc area centre candidate.

For the second voting procedure we tried the Maximum Difference Method proposed in [1]. But good results were obtained with an approach derived from this one. As in [1], a 21×21 median filter was applied on the green channel of the input image to eliminate isolated peaks. Then for each (i,j) pixel of the filtered green channel $I(x,y)$ the difference between the maximum grey value and minimum grey value of the pixels inside a 21×21 window centred on the current (i,j) pixel is calculated:

$$Diff(i,j) = I_W^{\max}(i,j) - I_W^{\min}(i,j). \tag{2}$$

There are stored four pixels with the greatest values $Diff(i,j)$. Then, starting from texture operators:

$$\begin{aligned} L5 &= \begin{bmatrix} 1 & 4 & 6 & 4 & 1 \end{bmatrix}, \\ E5 &= \begin{bmatrix} -1 & -2 & 0 & 2 & 1 \end{bmatrix}, \\ S5 &= \begin{bmatrix} -1 & 0 & 2 & 0 & -1 \end{bmatrix}, \end{aligned} \tag{3}$$

where:

$L5$ – mask to assess the grey level average;

$E5$ – edge mask;

$S5$ – corner mask,

the following masks, as in [8], are synthesized:

$$L5^t xE5 = \begin{bmatrix} -1 & -2 & 0 & 2 & 1 \\ -4 & -8 & 0 & 8 & 4 \\ -6 & -12 & 0 & 12 & 6 \\ -4 & -8 & 0 & 8 & 4 \\ -1 & -2 & 0 & 2 & 1 \end{bmatrix},$$

$$L5^t xS5 = \begin{bmatrix} -1 & 0 & 2 & 0 & 1 \\ -4 & 0 & 8 & 0 & 4 \\ -6 & 0 & 12 & 0 & 6 \\ -4 & 0 & 8 & 0 & 4 \\ -1 & 0 & 2 & 0 & 1 \end{bmatrix},$$

$$E5^t xL5 = \begin{bmatrix} -1 & -4 & -6 & -4 & -1 \\ -2 & -8 & -12 & -8 & -2 \\ 0 & 0 & 0 & 0 & 0 \\ 2 & 8 & 12 & 8 & 2 \\ 1 & 4 & 6 & 4 & 1 \end{bmatrix}, \tag{4}$$

$$S5^t xL5 = \begin{bmatrix} -1 & -4 & -6 & -4 & -1 \\ 0 & 0 & 0 & 0 & 0 \\ 2 & 8 & 12 & 8 & 2 \\ 0 & 0 & 0 & 0 & 0 \\ -1 & -4 & -6 & -4 & -1 \end{bmatrix}.$$

For each pixel of the filtered green channel $I(x, y)$ the texture parameter $f(i, j)$ is computed:

$$f(i,j) = \tag{5}$$

$$\sqrt{(f_{L5^t xE5}(i,j))^2 + (f_{L5^t xS5}(i,j))^2 + (f_{E5^t xL5}(i,j))^2 + (f_{S5^t xL5}(i,j))^2}.$$

The value $f(i, j)$ is then normalized:

$$F(i,j) = \frac{f(i,j) - f_{\min}}{f_{\max} - f_{\min}}, \tag{6}$$

where $f_{\max} = \max\{f(i,j)\}$, $f_{\min} = \min\{f(i,j)\}$, $0 \le i \le H-1$, $0 \le j \le W-1$, H is the image height and W is the image width.

From the four pixels with the greatest values $Diff(i, j)$ selected in the first stage it is retained the one with the largest average of $F(i, j)$ computed on the 21×21 window centred on the processed pixel.

From our tests we concluded that on the retinal images of healthy patients or in the early stages of affection this second voting method provides a closer point to the real optic disc centre than the first one. However, on the retinal images strongly affected it fails. Finally, if the two methods to approximate the optic disc centre provide close centres, it is chosen the one computed by the second method. Otherwise the centre computed by the first method is chosen. The results obtained with the two procedures are illustrated in Figure 1, where the little cross is the point found out by maximum difference method and the big cross is the point provided by the second algorithm.

In a second step, we tried to apply the same methodology on images of resolution 2592×1728 [12]. Good optic disc area localization results were obtained only with the Low-Pass Filter Method (1), the third method of the voting procedure in [1].

Results of detecting approximate optic centre position by two voting procedures for low resolution image are illustrated by Figures 2.a and 2.b. A result using Low-Pass Filter Method for high resolution image is depicted in Figure 2.d.

The optic disc zone identification using the same voting procedure as in [12] failed for a third set of retinal images, of resolution 720×576, provided by our collaborators from a different acquisition system. In the new set, the green channel was not always consistent in term of contrast. For some images the red channel is more suited to locate the optic disc area, for other ones the green channel is desirable.

The right channel selection was done using a square window scanning the whole red and green channels. The pixel intensity variance of the scanning window centre was computed. The window side length is the maximum expected circle diameter, estimated as a fraction of image width. The channel with the greatest maximum variance was chosen as working image to locate the optic disc area.

To identify the optic disc area in the selected image a new method was proposed [13]: the image was transformed in frequency domain

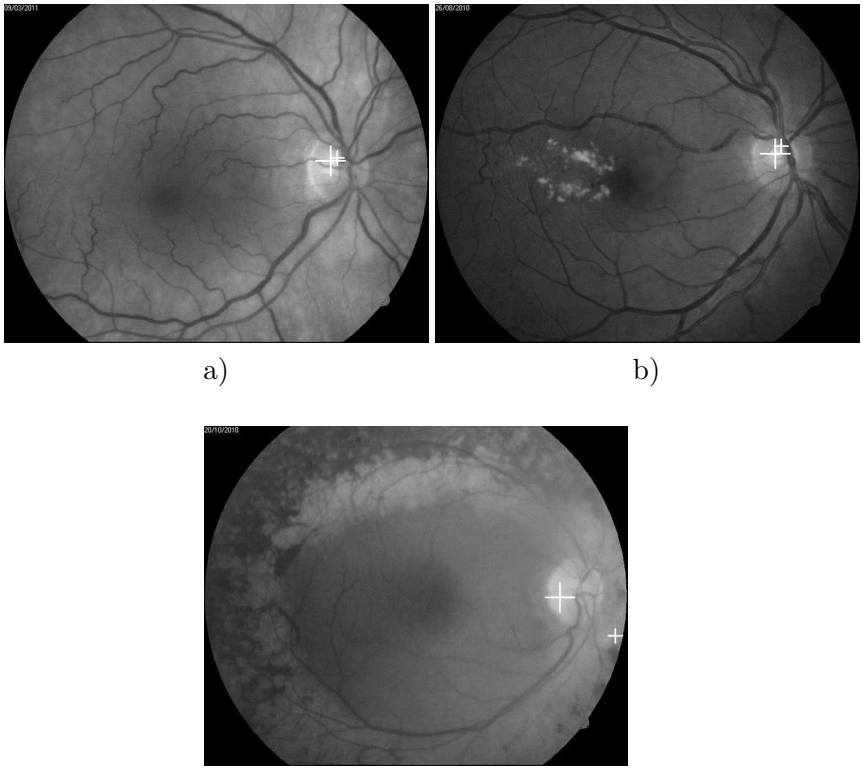

a) b)

c)

Figure 1. Results of detecting approximate optic centre position by two voting procedures. Point marked with little cross is provided by the first method and the one indicated by large cross is computed by the second voting algorithm. When the two points are far apart, as in the c) image, the centre computed by the first method is chosen – [11].

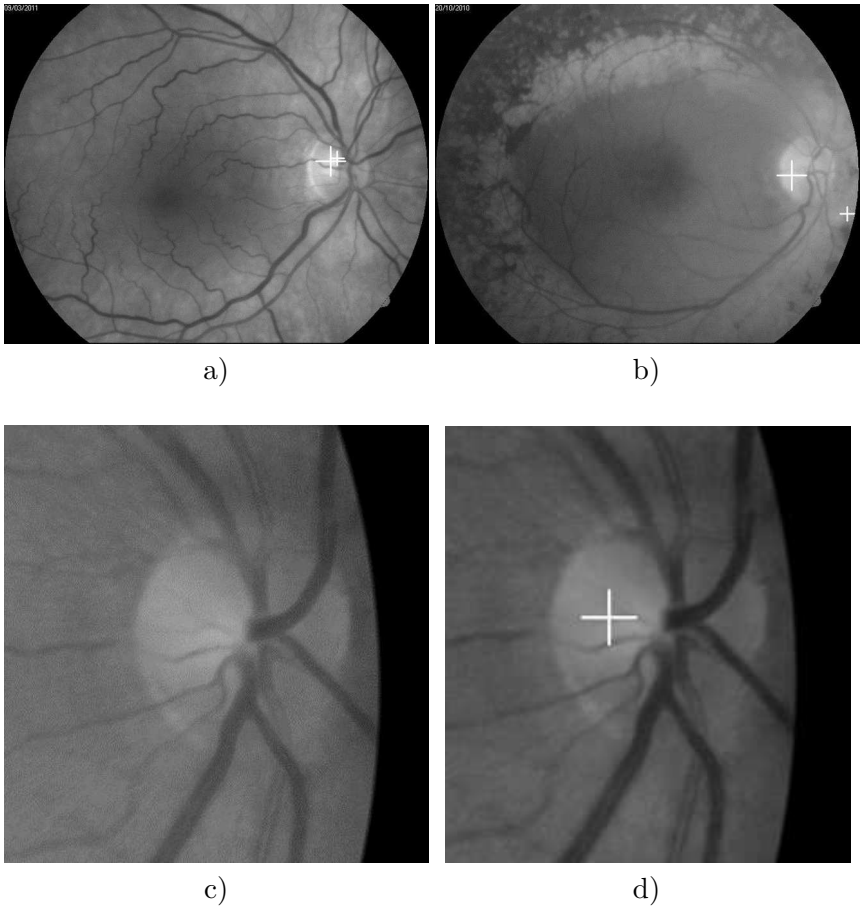

Figure 2. Results of detecting approximate optic centre position by two voting procedures for low resolution image, figures a) and b). Point marked with little cross is provided by the first method and the one indicated by large cross is computed by the second voting algorithm. When the two points are far apart, as in the b) image, the centre computed by the first method is chosen. A result using Low-Pass Filter Method for high resolution image is depicted in figure d). Part of original high resolution image is illustrated in figure c) – [12].

and the magnitude result of the FFT transform was filtered by Gaussian low-pass filter (1). The filtered result was transformed back to the spatial domain. Using the histogram of the new image, noted $I(i,j)$, a binarization threshold was computed. On each "bright" pixel (having a grey value greater than the binarization threshold) a square window of the same dimension as the one used in the channel selection step was centred. Then for every window centred in the "bright" pixels, intensity pixel variance, noted $Var(i,j)$, was calculated. Also, for every pixel $I(i,j)$ a texture measure was computed, using the same technique, Modified Maximum Difference Method, presented at the beginning of paragraph 2. A new image $F(i,j)$, of normalized texture values, was created. Finally, the pixel $O(m,n)$ of image $I(i,j)$ with $F(m,n) > \underset{\substack{0\le i\le H-1\\ 0\le j\le W-1}}{F(i,j)}$ and $Var(m,n) > 0.7max(Var(i,j))$ was declared as the centre of a window containing the optic disc.

Results of the new identification optic disc area procedure are depicted in Figure 3. The original image is 3.a. The images $I(i,j)$ and $F(i,j)$ are illustrated by Figures 3.b and 3.c. Black pixels in Figure 3.c are "dark" pixels of $I(i,j)$ not considered as possible optic disc centre candidates. The final result is depicted in Figure 3.d, where the cross indicates the centre of the working window in the selected channel.

Our previous methods to identify and model the optic disc provided very good results on retinal images of patients in early stages of ophthalmic pathologies as diabetic retinopathy or glaucoma. Tests have been made on three databases provided by our collaborators from UMP, Iaşi. We obtained good results also on images seriously affected by ophthalmic pathologies [12], [13].

The method proposed in [13] was tested on more than 100 images from STARE database of an image selection based on optic disc visibility. The results were good on the majority of these images but on other ones the optic disc was not correctly localized. Another method to segment the optic disc area was implemented based on the main blood vessels convergence point identification in the green channel.

Based on a technique employed from [6], in a first step the vessel tree of the green channel was iteratively segmented. A line of 27 pixels

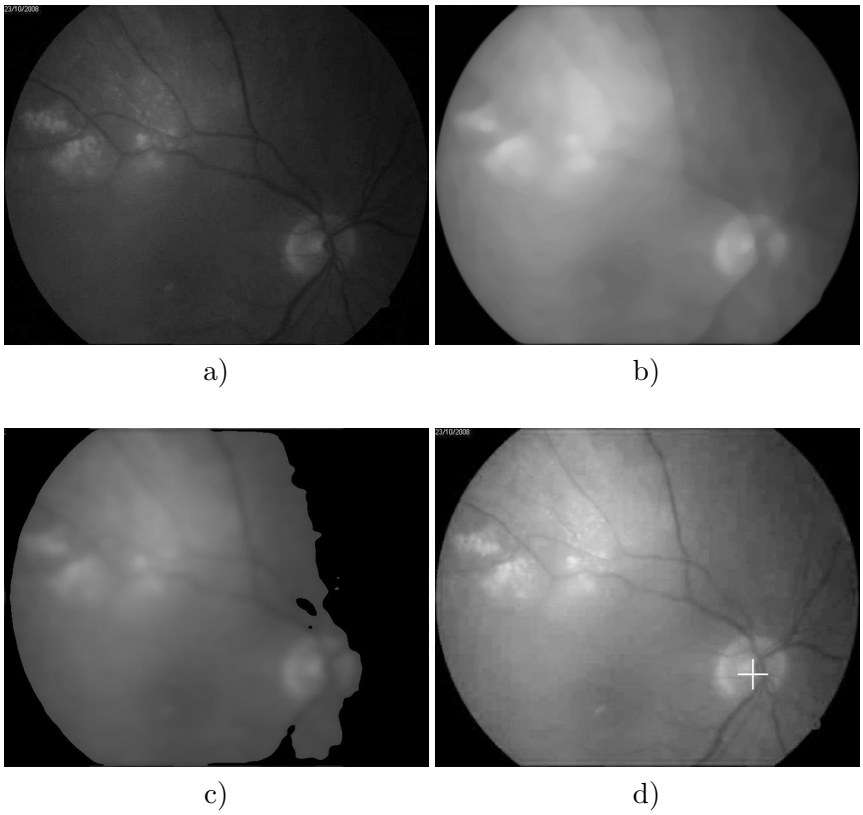

Figure 3. Result of detecting approximate optic centre position. a) Original RGB image; b) Gaussian filtering result in frequency domain $I(i,j)$; c) $F(i,j)$ image, where black pixels are "dark" pixels of $I(i,j)$; d) the cross indicates the working window centre – [13].

length and 1 pixel width was used as structuring element for an opening operation applied on the green channel for 12 different orientations of the element:

$$I_C = \min_{i=1,...12} \left(\gamma_{B_i}(I)\right), \tag{7}$$

where I is the input image, B_i is the structuring element and $\gamma_{B_i}(I)$ is the result of the opening for orientation i of the structuring element.

Then, using I_C as marker image and the green channel as mask image a morphological reconstruction was performed:

$$I_C = R_I\left(\underset{i=1,...12}{min}\left(\gamma_{B_i}(I)\right)\right). \tag{8}$$

An image containing only background (large homogenous areas) results from:

$$I_B = \underset{i=1,...12}{max}\left(\gamma_{B_i}(I)\right). \tag{9}$$

Subtracting I_B from I_C an image containing only blood vessels is generated:

$$I_V = I_C - I_B. \tag{10}$$

Then an Otsu binarization of the I_V image is iteratively applied until one of the vessel configurations is obtained: a) a vessel tree with a big ratio (number of white pixels)/(surrounding tree rectangle area) and with surrounding tree rectangle area at least half of the input image; b) two big vessel branches as illustrated in Figure 4; c) a single large branch with a low ratio (number of white pixels)/(surrounding tree rectangle area) but with surrounding tree rectangle area at least half of the input image.

For cases b) and c) the principal axis of the binarized vessels is computed. A search region is computed considering the distances to principal axis of the endpoints of the branches in two branch case or of the distances to principal axis of the parabola points in case c).

For configuration a) the search area was considered the minimum surrounding rectangle. The search area for case b) is illustrated in Figure 5.

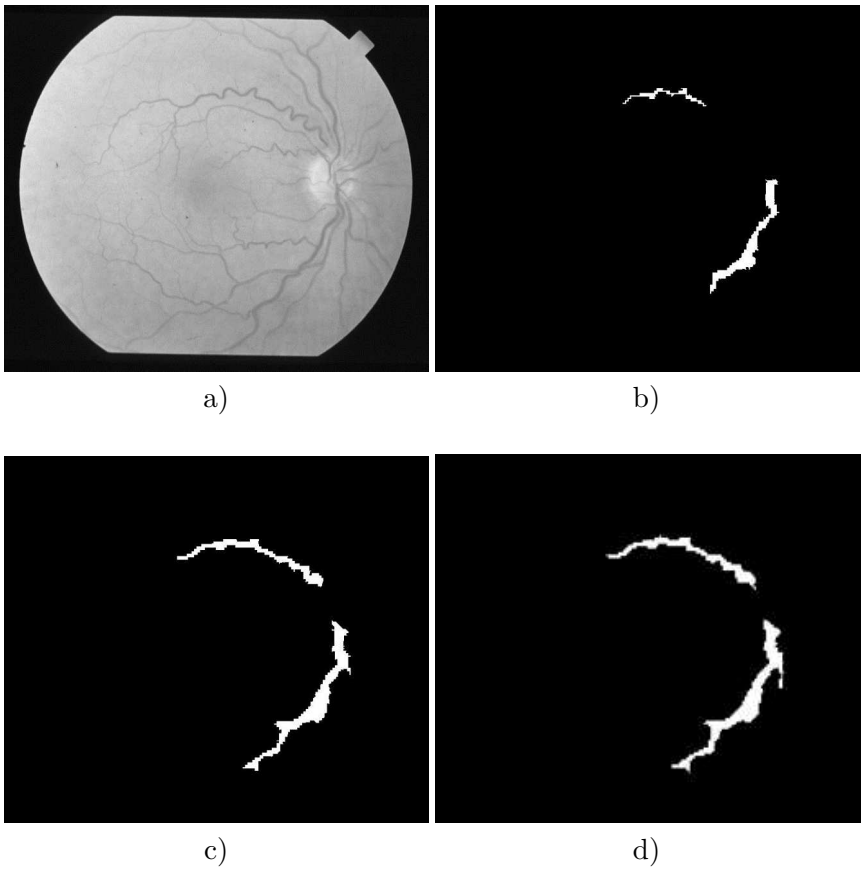

Figure 4. Results of I_V image binarization for two branch case. a) Original image; b) first step binarization; c) second step binarization; d) final step binarization.

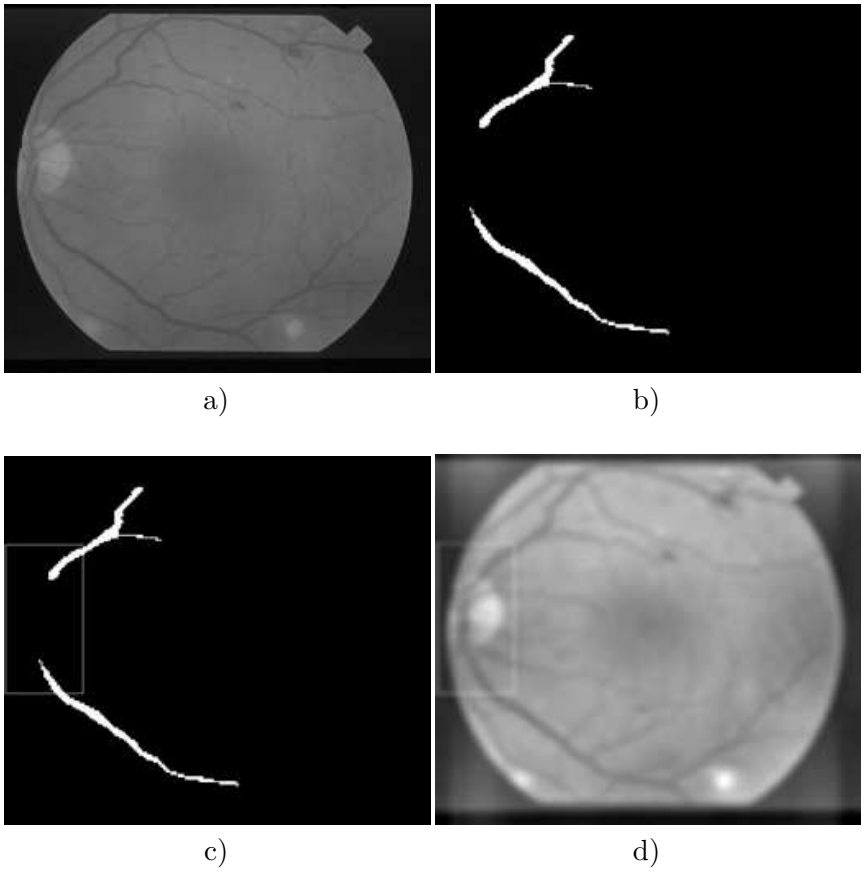

Figure 5. Search region for two branch case. a) original image; b) two final branches; c) search region in the working image; d) search region in the green channel were the next step is to approximately find the disc centre.

On the area established above, except of the FFT transform and Gaussian filtering, the procedure proposed in [13] was applied to identify a point to be declared the centre of a new window containing the optic disc.

Results of the new window centre calculation are depicted in Figure 6.

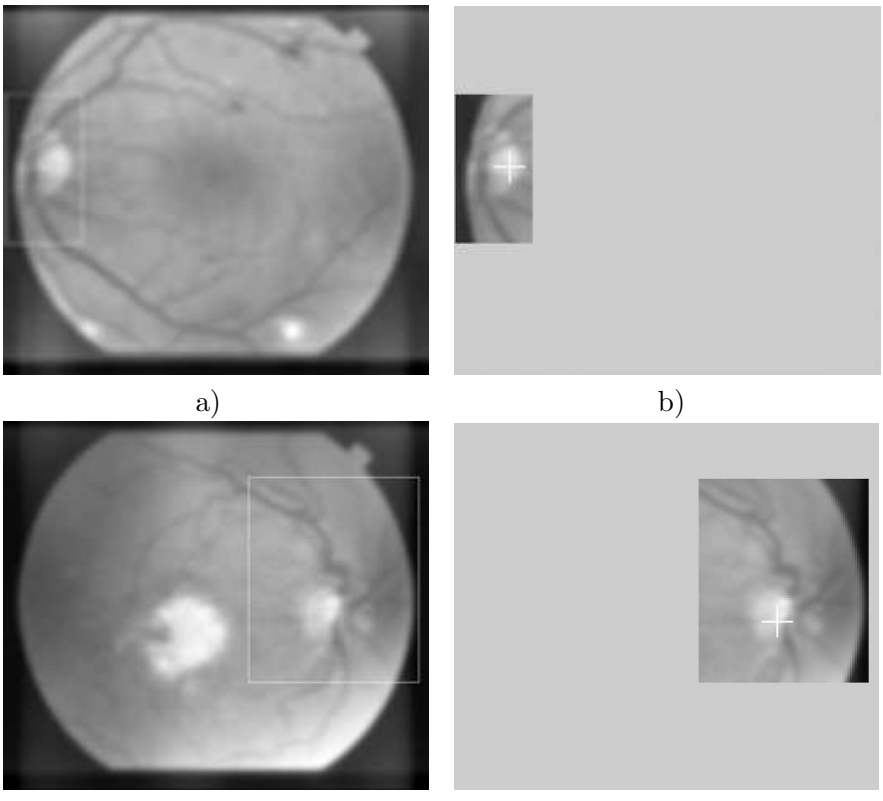

Figure 6. Results of the new window centre calculation. Green channels a), c); new window centre b), d).

3 Optic disc recognition

As in [1], [11], [12] and [13] the further work was done on a square window centred on the optic centre candidate computed previously. The searching window side is a fraction of image height. The tests have been done on the green channel of the first two sets of retinal images (86 retinal images of 720×576 size and 40 images of 2592×1728 resolutions), on chosen channel of the last set (300 of RGB retinal images of 720×576 size) from our collaborators (UMP, Iaşi) and on 100 images from STARE database where the optic disc is visible.

Following the same technique employed in [6] in the established window I the blood vessels were eliminated (7).

Results of the vessels erasing operation are illustrated by Figure 7, for last set of retinal images received from our collaborators (UMP, Iaşi).

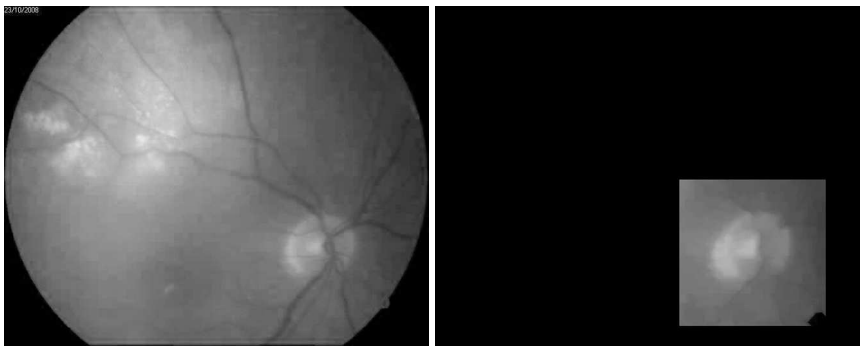

a) b)

Figure 7. The result of vessels erasing. a) Selected channel b) Cleaned working window – [13].

In order to perform a circle fitting the disc, edges have to be extracted. This is done by applying on image I_C an iterative Canny filter followed by binarisation. The same technique proposed in [12] and [13]

was employed to do this:

1. Compute a binarization threshold using Otsu method, [9], on image I_C, without performing the binarization.

2. Choose a value close to Otsu threshold as a primary threshold for Canny filtering.

3. Perform Canny filtering.

4. If there are not enough white pixels (less than a predefined threshold) adapt the threshold for Canny filtering and resume process from step 3.

5. Compute $r_{\min}$ and $r_{\max}$, the minimum and maximum values of circles radius, as fractions of the original image width.

6. For an interval $[r_{\min}, r_{\max}]$ of circle radius compute a circle fitting by Hough transform applied on window pixels with grey level close to the window centre level.

7. Choose the centre radius with the best fitting score and best distribution of fitting points.

8. If the fitting score is not desirable or there are few points to perform the fitting, decrease the Canny threshold by a certain amount (constant in our implementation) and perform Canny filtering on I_C and resume the process from step 6. Do this not more than a predefined number of iterations.

9. If the detected circles have comparable fitting scores and fitting point distributions, choose the circle with the longest radius.

Canny filtering was done using the OpenCV function. Hough transform was performed by implementing our own method in order to get more control on the distribution of the fitting points [12], [13]. The distance between the current fitted circle centre and the mass centre of the fitting points was used to evaluate the point distribution. In

this way some configurations can be rejected even they are generated by an acceptable number of fitting points if the points are not equally distributed around circle centre.

4 Results and conclusions

Tests have been done on two first sets of 86 RGB retinal images of 720×576 resolution and 40 images of 2592×1728 resolution provided by our collaborators (UMP, Iaşi). The method [13] to detect the optic disc area worked well, with the same results as the one presented in [12]: the rough optic disc localization has been successful on both image sets. The final circle fitting failed on two low resolution images strongly affected. Because the previous method [12] is faster we opted to keep it for the old sets and use the approach presented in [13] only for the last set of 300 retinal images of 720×576 resolution. The optic disc localization has been successful on 280 images of the last set. The final circle fitting failed on 10 images of the 280 images previously mentioned.

The last method based on vessel tree analysis was tested on the set of 300 RGB retinal images of 720×576 size provided lately by our collaborators (UMP, Iaşi) and on 100 images from STARE database where the optic disc is visible. The new optic disc localization has been successful on 282 images of the first set, a little bit better than the previous method [13]. However, from 100 images chosen from STARE database the method [13] failed to localize to optic disc area on 20 images while the new method was successful on 90 STARE images.

Figure 8 illustrates some final circle localization results for images from the three sets from Grigore T. Popa University of Medicine and Pharmacy Iasi and an image from STARE database.

The optic disk localization and modelling procedure was implemented and tested in an image processing framework developed by authors. It is implemented as a Windows application, in C++ using Microsoft Visual Studio. For image manipulation and some processing functions, the OpenCV library is used.

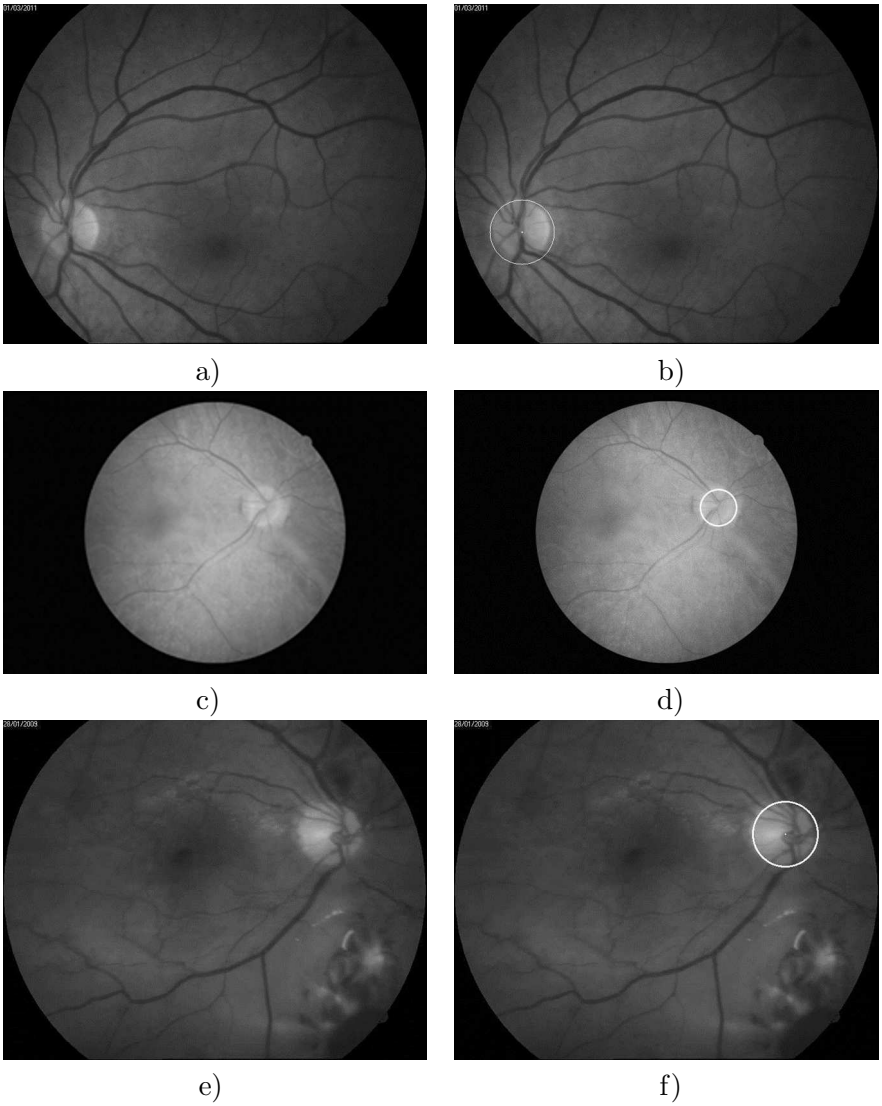

a) b)

c) d)

e) f)

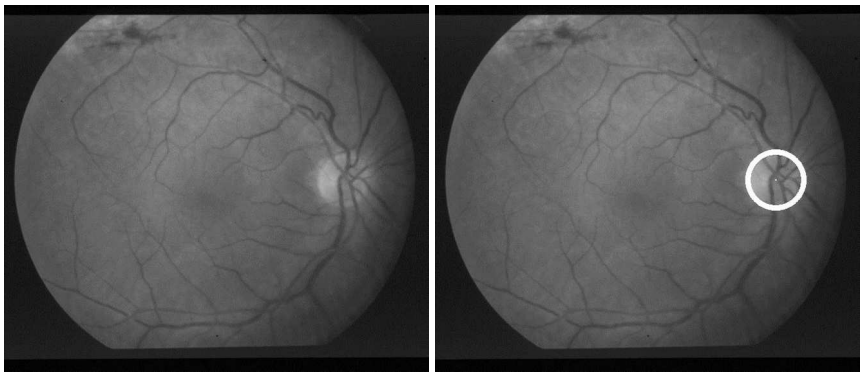

g) h)

Figure 8. On the left column: original retinal images. On the right: the final optic disc localization results. a), b) image from the first set of 720×576 resolution – [11]; c), d) image from the set of 2592×1728 resolution – [12]; e), f) image from the last set of 720×576 size – [13]; g), h) image from the STARE.

Acknowledgments The work was done as part of research collaboration with Grigore T. Popa University of Medicine and Pharmacy Iasi to analyse retinal images for early prevention of ophthalmic diseases.

References

[1] A. Aquino, M.E. Gegundez-Arias, D. Marin. *Detecting the optic disc boundary in digital fundus images using morphological, edge detection, and feature extraction techniques*, IEEE Transactions on Medical Imaging, Nov. 2010, Volume 29, Issue 11, pp.1860–1869.

[2] B. Harangi, A. Hajdu. *Improving the accuracy of optic disc detection by finding maximal weighted clique of multiple candidates of individual detectors*, IEEE 9th International Symposium on

Biomedical Imaging (ISBI2012), Barcelona, Spain, 2012, pp.602–605.

[3] B. Harangi, R.J. Qureshi, A. Csutak, T. Peto, A. Hajdu. *Automatic detection of the optic disc using majority voting in a collection of optic disc detectors*, IEEE 7th International Symposium on Biomedical Imaging (ISBI 2010), Rotterdam, The Netherlands, 2010, pp.1329–1332.

[4] H.Li, O. Chutatape. *Automated feature extraction in color retinal images by a model based approach*, IEEE Transactions on Biomedical Engineering, Vol.51, No.2, February 2004.

[5] A. Hoover, M. Goldbaum. *Locating the optic nerve in a retinal image using the fuzzy convergence of the blood vessels*, IEEE Trans. Med. Imag., vol. 22, no. 8, pp.951–958, Aug. 2003.

[6] C. Heneghan, J. Flynn, M. O'Keefe, M. Cahill. *Characterization of changes in blood vessel width and tortuosity in retinopathy of prematurity using image analysis*, Med. Image Anal., vol. 6, pp.407–429, 2002.

[7] M. Foracchia, E. Grisan, A. Ruggeri. *Detection of optic disc in retinal images by means of a geometrical model of vessel structure*, IEEE Trans. Med. Imag., vol. 23, no. 10, pp. 1189–1195, Oct. 2004.

[8] M. Lalonde, M. Beaulieu, L. Gagnon. *Fast and robust optic disk detection using pyramidal decomposition and Hausdorff-based template matching*, IEEE Trans. Medical Imaging, Vol. 20, pp. 1193–1200, Nov. 2001.

[9] N. Otsu. *A threshold selection method from gray-level histograms*, IEEE Transactions on Systems, Man, and Cybernetics, Vol. 9, No. 1, 1979, pp. 62–66.

[10] S. Ravishankar, A. Jain, A. Mittal. *Automated feature extraction for early detection of diabetic retinopathy in fundus images*, CVPR – IEEE Conference on Computer Vision and Pattern Recognition, pp. 210–217, 2009.

[11] F. Rotaru, S. Bejinariu, C.D. Niţă, M. Costin. *Optic disc localization in retinal images*, 5th IEEE International Workshop on Soft Computing Applications, 23-25 August, 2012, Szeged, Hungary, Soft Computing Applications – Advances in Intelligent Systems and Computing Volume 195, 2013, Springer Verlag.

[12] F. Rotaru, S. Bejinariu, C.D. Niţă, R. Luca. *New optic disc localization method for retinal images*, IEEE International Symposium on Signal, Circuits and Systems, ISSCS 2013, 11-12 July 2013, Iasi, Romania.

[13] F. Rotaru, S. Bejinariu, C.D. Niţă, R. Luca, C. Lazăr. *New optic disc localization approach in retinal images*, The 4^{th} IEEE International Conference on E-Health and Bioengineering, EHB 2013, 21-23 November 2013, Iasi, Romania.

[14] A. Sopharak, K. Thet Nwe, Y. Aye Moe, M. N. Dailey, B. Uyyanonvara. *Automatic exudate detection with a naive Bayes classifier*, International Conference on Embedded Systems and Intelligent Technology, Grand Mercure Fortune Hotel, Bangkok, Thailand, pp.139–142, 2008.

[15] G.C. Manikis, V. Sakkalis, X. Zabulis, P. Karamaounas, A. Triantafyllow, S. Douma, Ch. Zamboulis, K. Marias. *An Image Analysis Framework for the Early Assessment of Hypertensive Retinopathy Signs*, Proceedings of the 3rd IEEE International Conference on E-Health and Bioengineering - EHB 2011, 24th-26th November, 2011, Iaşi, Romania.

[16] Yanhui Guo. *Computer-Aided Detection of Breast Cancer Using Ultrasound Images*, PhD Thesis, Utah State University, 2010.

[17] D. Welfer, J. Scharcanski, C.M. Kitamura, M.M. DalPizzol. *Segmentation of the optic disk in color eye fundus images using an adaptive*, Comput Biol Med, vol. 40, no. 2, pp. 124–137, 2010.

[18] K.W. Tobin, E. Chaum, V.P. Govindasamy, T.P. Karnowski. *Detection of anatomic structures in human retinal imagery*, IEEE Transactions on Medical Imaging 26 (12) (2007), pp.1729–1739.

[19] M. Park, J.S. Jin, S. Luo. *Locating the optic disc in retinal images*, Proceedings of the International Conference on Computer Graphics, Imaging, and Visualisation, IEEE, Sydney, Australia, 2006, pp.14–145.

[20] C. Sinthanayothin, J.F. Boyce, H.L. Cook, T.H. Williamson. *Automated localisation of the optic disc, fovea, and retinal blood vessels from digital colour fundus images*, British Journal of Ophthalmology 83 (1999), pp.902–910.

[21] A.A.-H.A.-R. Youssif, A.Z. Ghalwash, A.A.S.A.-R. Ghoneim. *Optic disc detection from normalized digital fundus images by means of a vessels' direction matched filter*, IEEE Transactions on Medical Imaging 27 (1) (2008) pp.11–18.

[22] J. Lowell, A. Hunter, D. Steel, A. Basu, R. Ryder, E. Fletcher, L. Kennedy. *Optic nerve head segmentation*, IEEE Transactions on Medical Imaging 23 (2) (2004), pp.256–264.

[23] M. Niemeijer, M.D. Abramoff, B.V. Ginneken. *Segmentation of the optic disc macula and vascular arch in fundus photographs*, IEEE Transactions on Medical Imaging 26 (2007), pp.116–127.

[24] A.D. Fleming, K.A. Goatman, S. Philip, J.A. Olson, P.F. Sharp. *Automatic detection of retinal anatomy to assist diabetic retinopathy screening*, Physics in Medicine and Biology 52 (2) (2007), pp.331–345.

[25] E.J. Carmona, M. Rincon, J. Garcıa-Feijoo, J.M.M.de-la Casa. *Identification of the optic nerve head with genetic algorithms*, Artificial Intelligence in Medicine 43 (3) (2008), pp.243–259.

[26] C.A. Lupascu, D. Tegolo, L.D. Rosa. *Automated detection of optic disc location in retinal images*, in: 21st IEEE International Sym-

posium on Computer-Based Medical Systems, IEEE, University of Jyvaskyla, Finland, 2008, pp. 17–22.

[27] T. Walter, J.-C. Klein, P. Massin, A. Erginay. *A contribution of image processing to the diagnosis of diabetic retinopathy—detection of exudates in color fundus images of the human retina*, IEEE Transactions on Medical Imaging, 21 (10) (2002), pp.1236–1243.

[28] A. Sopharak, B. Uyyanonvara, S. Barman, T.H. Williamson. *Automatic detection of diabetic retinopathy exudates from non-dilated retinal images using mathematical morphology methods*, Computerized Medical Imaging and Graphics, 32 (2008), pp.720–727.

Florin Rotaru, Silviu Ioan Bejinariu,
Cristina Diana Niţă, Ramona Luca, Camelia Lazăr

Received June 2, 2014

Institute of Computer Science, Romanian Academy,
Iasi Branch, Romania
E–mails: {*florin.rotaru, silviu.bejinariu, cristina.nita, ramona.luca, camelia.lazar*}@
iit.academiaromana-is.ro